54th CIRP Conference on Manufacturing Systems

# Genetic algorithm for the optimization of vision acquisition for on-the-fly position measurement of individual layers in fuel cell stack assembly

Jens Schäfer[a],*, Simeon Allmendinger[a], Janna Hofmann[a], Jürgen Fleischer[a]

*a*wbk Institute of Production Science, Karlsruhe Institute of Technology, Kaiserstraße 12, 76131 Karlsruhe, Germany

* Corresponding author. Tel.: +49-1523-9502613; *E-mail address:* jens.schaefer@kit.edu

**Abstract**

Polymer electrolyte membrane (PEM) fuel cells consist of hundreds of stacked individual layers. As misplacement can lead to product-malfunctions the positioning accuracy plays a crucial role during assembly. Thus, to increase accuracy and to lower the cycle time, this paper presents a camera-integrated gripper for single layer handling of fuel cell components. The overlapping of suction holes within a gripper system is used for position measurement of fuel cell layers. The hole pattern is optimized applying a genetic algorithm to precisely measure the position of individual layers.

## 1. Motivation

Polymer electrolyte membrane (PEM) fuel cells have the potential to reduce carbon footprint, especially in heavy duty applications. Although fuel cells have been in development for decades, the quantity stayed rather small, thus being assembled manually most of the time. Along with a rising demand for fuel cells due to emission regulations the need for automated production machines rises. A key process in fuel cell production is the stacking of individual parts, which needs to be very precise on the one hand but also fast on the other hand. Hence the use of vision guided assembly is inevitable.

## 2. State of the art

### 2.1. PEM Fuel cell stacks

PEM fuel cell stacks are composed of up to hundreds of individual cells [1,2]. The basic structure of a single cell is shown in Fig. 1.
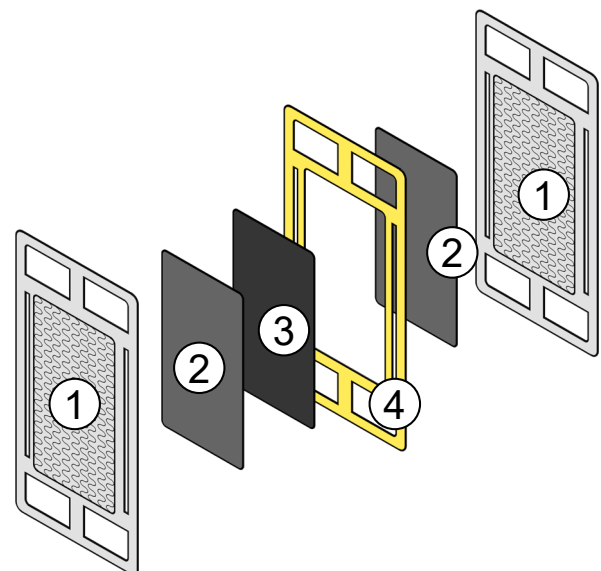


Fig. 1. Components of a fuel cell (1) bipolar plate (2) Gas diffusion layer (GDL) (3) Catalyst coated membrane (CCM) (4) Subgasket

Each cell features a bipolar plate (1), a catalyst coated membrane (3, CCM) sandwiched between two gas diffusion layers (2, GDL) followed by the next bipolar plate (1). Sealing concepts vary between different manufacturers, so do concepts for pre-assembled parts. Commonly the GDL's and CCM are assembled to a so-called membrane electrode assembly (MEA). This can either be achieved roll-to-roll by laminating onto a subgasket [3] or by pick and place operations with a GDL, where the sealing is applied at the edges [4]. The components feature high variance in material properties such as Young's modulus, thickness and gas-permeability [5].

Alternating stacking of bipolar plate and MEA form a fuel cell stack, which is then compressed and fixed, ensuring gas tightness and a lower resistance in the fuel cell active area. For a functioning fuel cell stack the gas tightness is crucial and the alignment during compression has to be ensured. This leads to high requirements regarding the stacking accuracy. As automotive stacks usually have hundreds of individual layers stacking can create a bottleneck in fuel cell stack production.

## 2.2. Production technology for fuel cell stacks

Due to their flexibility vision guided kinematics are broadly used in manufacturing systems. In addition to simple position determination their use also extends to the detection of faulty parts and general quality assurance [6]. Vision technology in fuel cell production and stacking of fuel cell components in specific have only been scientifically discussed to a limited extend. An AI-supported approach based on a multi camera structure is described in [1,2]. Cameras detect and compare the position of individual components before and after grasping. It was stated, that a large fraction of the measured inaccuracy is caused by the gripper itself, which was not in the scope of the investigations. Another handling system is presented in [7], due to the necessity of alignment pins the stack size is limited and it can hardly be applied for automotive fuel cell stacks. Another robot based system is presented in [4]. The applied positioning system and the method for grasping however is not specified.

## 3. Own approach

### 3.1. Framework conditions

A production system for fuel cell stacking has to be both, precise and fast. Due to the limp layers the alignment of the components has to be carried out through visual position measurement. The most accurate measurement can be obtained when measuring the component position relative to the gripper whilst grasping. However, if done by an external camera the handling unit needs to move to the designated position and might even need to stop, which would increase cycle time. A gripper integrated measurement system that is capable of measuring the position whilst handling can reduce cycle time and increase accuracy. Fig. 2 shows the characteristic traits for position measurement of the components A) MEA, B) CCM and C) bipolar plate at their edges. The CCM is a flat component which might additionally have rounded edges, MEA and bipolar plate in addition feature cut-outs.
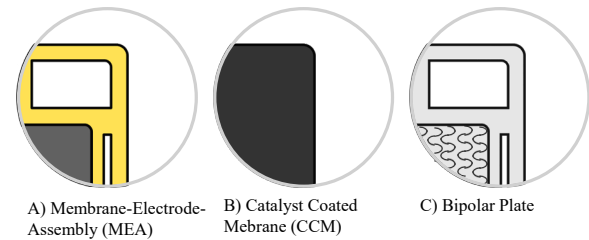


Fig. 2. Characteristic traits of fuel cell components

A) Membrane-Electrode-Assembly (MEA)    B) Catalyst Coated Mebrane (CCM)    C) Bipolar Plate

Different characteristics such as the component centre point can be used to determine the overall component position in a predefined coordinate system. However, when shifting along the axis and rotating around the centre point of a rectangular object, the displacement will be greatest in one of its corners. Since this aspect gains relevance with the sealing applied at the edges a conclusive measurement point defined by one corner is more meaningful. For this reason, position accuracy in this paper will be described as the difference of the component edge of the nominal and the actual position as described in Fig. 3.
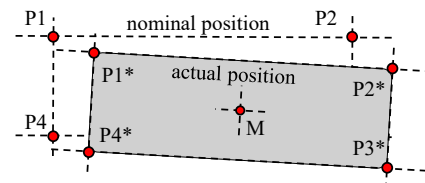


Fig. 3. Definition of positions

An in-process position measurement requires an integration of sensors into the gripper in a hand-eye configuration. Most favourable are optical 2D-sensors as they can measure all degrees of freedom and are less sensitive for selective deviations compared to 1D Sensors. For the integration, however, several constraints exist. The membrane is very thin, thus complete area gripping is necessary in order to prevent sagging. Sealant applied to the GDL can adhere to the gripper, making anti-stick coating necessary. Low pressure surface grippers are well suited for handling, as they meet all the challenges. These grippers feature an integrated vacuum generator and a predetermined hole pattern. The suction holes are usually distributed evenly in reoccurring quadratic shapes with a grid constant, which is the aggravating factor for a position acquisition originating from the backside. In this approach a hole pattern is optimized to detect the position with an internal camera recording incoming light from the uncovered suction holes. This setup is illustrated in Fig. 4.



1 grasped object    3 camera
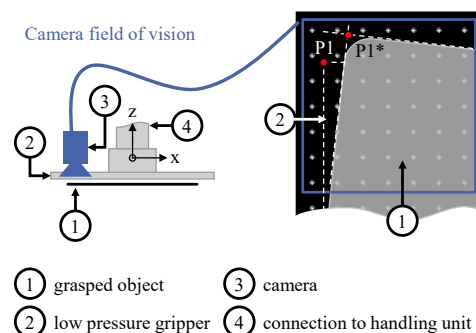2 low pressure gripper    4 connection to handling unit

Fig. 4. Gripper setup with integrated camera

In the gripper system the installation space is limited. Thus, the camera lens will have a small distance to the suction holes and can only capture a section of the layers in a limited field of vision. Considering the previously described accuracy requirements an image section is chosen which records the incoming light at one corner of the layer. For optimization there are three boundary conditions. Firstly, the distance between suction holes of the low-pressure vacuum gripper is defined by the mechanical stability of the gripper. It limits the achievable accuracy of a camera mounted on the backside as shown in Fig. 4. Secondly, the number of holes needs to remain constant, since an increase can cause high pressure losses for permeable materials, such as the GDL. Thirdly, the diameter of the suction holes is limited due to the deformation potential of layers through suction force, mainly for the very thin CCM. As a result, the objective is to increase the possible accuracy with a given number of holes and a fixed diameter.

### 3.2. Methodology

For the methodology the position definitions in Fig. 3 are extended by the calculated position, as shown in Table 1.

Table 1: Definition of nominal, actual, calculated position

| Term | Definition | Nomenclature |
|------|-----------|--------------|
| Nominal position | Describes the target position of the layer. | P |
| Actual position | Describes the real position of the layer. | P* |
| Calculated position | Describes the position of the layer, which is geometrically calculated using an algorithm. | $P_{Calc}$ |

Nature-inspired genetic algorithms offer the possibility to optimize a given pattern via selection, mutation and recombination of genes. The main advantage in deploying genetic algorithms is that their use is not dependent on a specific shape of the component and the methodology can thus be transferred to numerous other applications. The entirety of genes forms an individual representing a potential solution. One gene of an individual contains the x- and y- position value of a single suction hole. In order to attain a sufficient evaluation criterion for various patterns a fitness value is attributed to each solution. In this approach the fitness is defined by the difference between calculated position and actual position at a given corner point as described in equation (1). Three degrees of freedom – shift in x and y as well as rotation around z – are taken into account when evaluating the fitness. These parameters make an accurate description of the *calculated* and *actual* position possible.

$$\Delta P_k = \left\| \overrightarrow{P_k} - \overrightarrow{P_k^*} \right\|_2 = \sqrt{(x_k - x_k^*)^2 + (y_k - y_k^*)^2} \qquad (1)$$

The main goal is then to iteratively minimize the position acquisition error represented by the fitness value. Since small variations in lighting conditions of the assembling environment would severely affect the detection process a simplified model is applied. Thus, drawing conclusions on the actual position the algorithm differentiates between three types of suction holes: *A)* a hole being fully covered by the component *B)* a hole being

partly covered by the component and *C)* a hole not being covered by the component. The procedure for obtaining the illumination of the suction holes is shown in a schematic illustration in Fig. 5. Basically, the position of the corner is calculated with information on all three suction hole types *A, B, C*. The corner $P^*$ is then specified by weighting $P_A^*$, $P_B^*$ and $P_C^*$. In addition, this fundamental method includes several extensions and modifications considering more than only those illustrated holes. Consequently, the calculated position of the corner point P is more robust, as more points are used for position estimation.
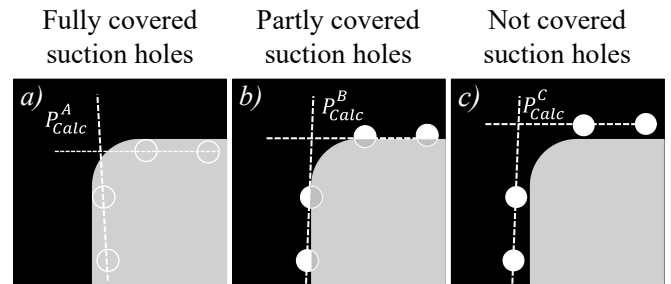


Fig. 5. Calculation of corner position within the image section

Optimizing the fitness, the algorithm makes use of three key ideas: selection, mutation, and combination. The general methodology is stated in [8,9]. In each iteration the best individuals are selected as parents, which then form the basis for mutated and recombined offspring creating a new set of patterns. For the selection of the individuals a combination of two different methods is implemented: elitism and fitness-proportional selection. These help to avoid local minima due to the modification of the selection pressure which fosters exploring in the beginning and increases exploitation in the end. A Gaussian distribution defines the mutation of genes (Gauss-Mutation) and the recombination is achieved through crossing of gene-strings at one point (1-Point-Crossover). If the fitness improvement is below a specific convergence threshold the algorithm determines. The initial hole pattern is arranged in quarter circles, as this has shown to enhance the possible measuring accuracy and therefore reducing computation time. The chosen values are shown in Table 2.

Table 2: Specifications used for the genetic algorithm

| Parameter | Value |
|-----------|-------|
| Hole size | 0.5 mm |
| Minimal distance between individual holes | 1.0 mm |
| Number of layer positions | 1000 |
| Individuals | 12 |
| Number of genes | 100 |
| Image section | 60 mm by 60 mm |

## 4. Results

Based on the pre-described methodology both layer types were investigated: CCM as well as MEA and bipolar plate *(cp. Fig. 2)*. First, 1000 random layer positions for the CCM were created. These simulated positions have the advantage, that the exact position as a reference is well known. The positions were allocated using a Gaussian distribution in all three degrees of freedom based on the desired nominal position. The evolution

of the suction hole pattern is exemplary shown in Fig. 6, starting from the first-generation a) until generation 601 d), where the algorithm terminated.
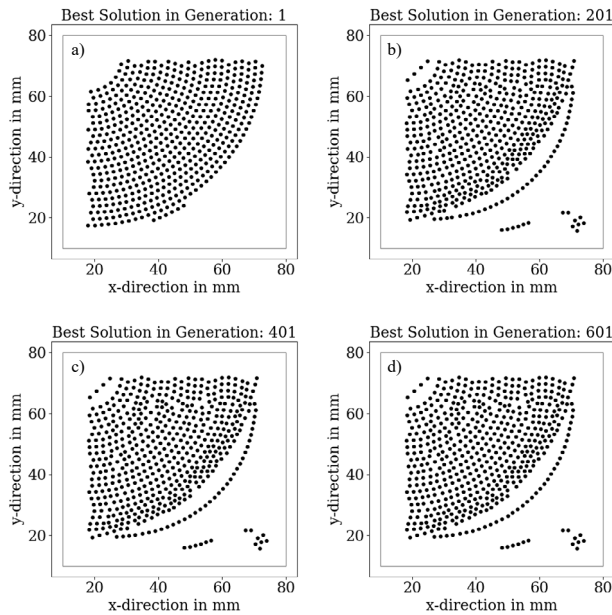


Fig. 6. Optimization behaviour of solution patterns

In later iterations there are outliers at the bottom right corner, which do not contribute to the position acquisition. They occur from recombination and do not find their way back in the main point cloud during optimization. Thus, points in this area can be neglected and are subsequently removed.

The graph in Fig. 7 displays the course of convergence for each generation with solutions a) – d) from Fig. 6. being labelled. The accuracy of the best solution pattern (blue) as well as the average (orange) regarding all solution patterns in each generation of above-mentioned example show a converging curve towards an optimum.
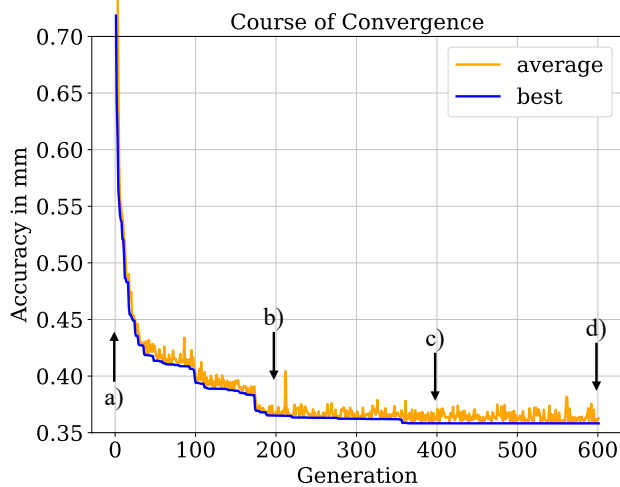


Fig. 7. Course of convergence – fitness values in each generation

Before discussing the achieved accuracy, it must be taken into account that in the genetic algorithm the accuracy was defined by the error of the corner furthest away from the camera field of vision, simulating the use of a single camera. This practice considers the maximum error. The histograms in

Fig. 8 show the achieved accuracy distribution of the corner point within the field of vision and the one furthest away from the field of vision for a CCM and an image section of 60 mm x 60 mm.
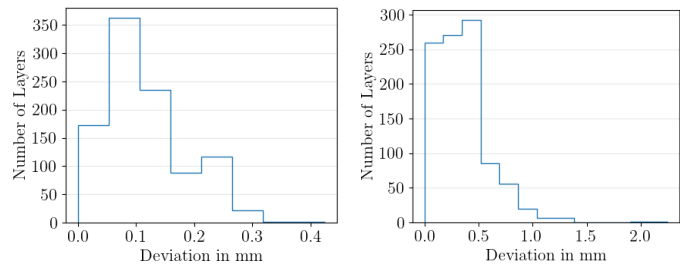


Fig. 8. Histograms showing the accuracy distribution among all 1000 layers for corner P1 (left) and P3 (right). Image section size: 60mm x 60mm

The illustration in Fig 8 underlines, that the accuracy of the furthest corner (P3$^*$) is considerably worse compared to the corner (P1$^*$) within the image section. The probability for correctly predicting a position of a corner point with a given accuracy in a 60 mm x 60 mm image section is shown in Table 3.

Table 3. Probability for correct identification of the actual position for desired accuracies

| desired accuracy | point | probability |
|---|---|---|
| 0.3 mm | P1* | 99.20 % |
| | P3* | 47.10 % |
| 0.5 mm | P1* | 100.00 % |
| | P3* | 75.8 % |

The effect of the image section size on the accuracy of 1000 randomly created positions of bipolar plates was investigated as well. In Fig. 9 six different sizes for the field of vision were considered ranging from 40 mm x 40 mm to 90 mm x 90 mm. The results show a relation between accuracy and image section size. It can be argued that the majority of layers is detected within a similar deviation interval regardless of the image section size – especially for an edge length above 40 mm. However, it should be recognised that the functionality of a single PEM fuel cell is only ensured, if all layers are stacked precisely and hence outliers cannot be neglected.
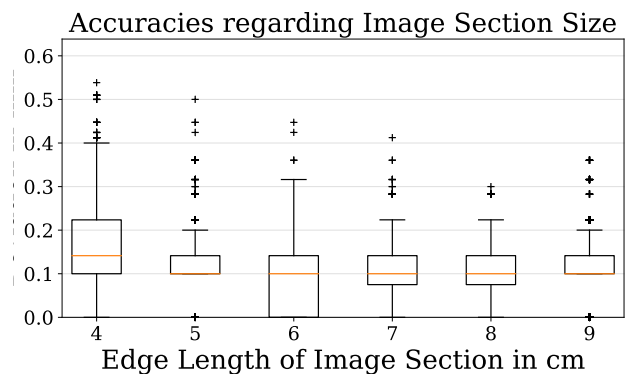


Fig. 9. Accuracy distribution for the corner P1 within the image section

There are mainly two reasons for this relation. First of all, with an enlarged image section the number of suction holes rises, which increases the information value regarding all three types of suction holes – fully (C), partly (B), not covered (A). Partly covered holes – right on the layer's edges – strongly refine the position acquisition, thus, having a larger number at hand strongly improves the accuracy. The second reason comes along with the first aspect. When measuring the rotation of the layer the angle error can be minimized due to more visible suction holes near the edges. As the contours are detected alongside a bigger distance the image section features a more precise picture of the rotation. Moreover, it is noteworthy to consider the median, which is mostly 0.1 mm. This is caused by the pixel size and the simplified assumption of three different suction hole types. However, this issue can be addressed when observing the differences in illumination of the suction holes more fine-tuned. The following solution pattern in Fig. 10 represents the results for the image section size of 90 mm x 90 mm.
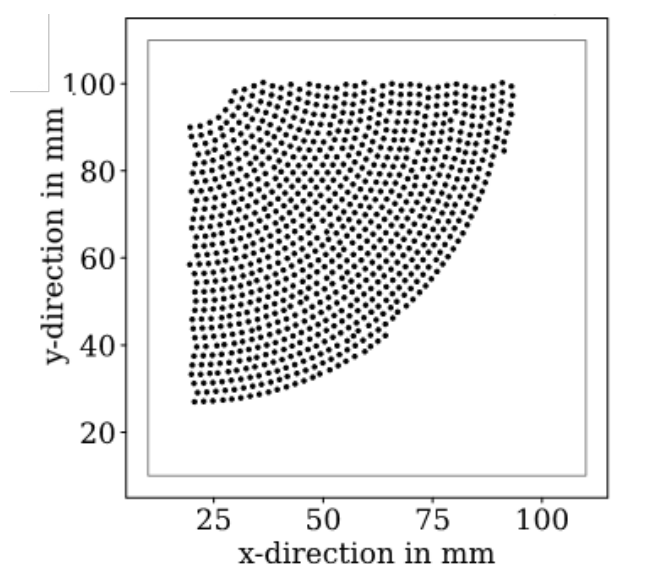


Fig. 10. Solution pattern Solution pattern for a 90 mm x 90 mm image section

## 5. Conclusion

In this paper particular attention has been paid to precisely stacking fuel cell components. The findings on the one hand show precise position acquisition for the corner P1 within the image section of 80 mm x 80 mm and 90 mm x 90 mm. A deviation interval between -0.3 mm and 0.3 mm is attained. On the other hand, the accuracy regarding the furthest corner is not sufficient for the stacking purpose. Therefore, the field of vision can be increased, for example by a multi-camera layout.

The distance between the suction holes and the camera is crucial due to limited installation space. However, it depends on the minimal image section size ensuring the accuracy target. It should be noted that camera specifications vary – such as the focal length – thus, general statements about a camera distance cannot be made. Theoretically, the bigger the distance, the better the accuracy. Conversely, the practice is dependent on several factors. On one hand, the position of the camera is limited by the mounting space within the gripper system. On the other hand, extremely wide-angle lenses lead to another problem in a real production environment. Incoming light from the outer suction holes has a very flat angle. As a consequence, the thickness of the perforated gripper plate reduces the field of vision.

## 6. Outlook

This paper demonstrates the use of a genetic algorithm for the optimization of a fuel cell gripper system. The findings encourage further efforts in this research area. Therefore, this work proposes the following future research steps with regard to series production. In following investigations a suction plate can be produced according to the best solution. On this basis, solutions can be validated allowing a statement regarding the accuracy for real conditions. The results have shown, that the position detection for the furthest point is poor, hence the approach can be transferred to a multi-camera system, covering a larger area of the gripper.

## 7. Acknowledgement

## References

[1] P. Bobka, F. Gabriel, M. Römer, T. Engbers, M. Willgeroth, K. Dröder, Fast Pick and Place Stacking System for Thin, Limp and Inhomogeneous Fuel Cell Components, in: J.P. Wulfsberg, W. Hintze, B.-A. Behrens (Eds.), Production at the leading edge of technology, Springer, Berlin, Heidelberg, 2019, pp. 389–399.

[2] P. Bobka, F. Gabriel, K. Dröder, Fast and precise pick and place stacking of limp fuel cell components supported by artificial neural networks, CIRP Annals 69 (2020). https://doi.org/10.1016/j.cirp.2020.04.103.

[3] J. Chen, H. Liu, Y. Huang, Z. Yin, High-rate roll-to-roll stack and lamination of multilayer structured membrane electrode assembly, Journal of Manufacturing Processes 23 (2016) 175–182. https://doi.org/10.1016/j.jmapro.2016.06.022.

[4] Porstmann, Wannemacher, Richter, Overcoming the Challenges for a Mass Manufacturing Machine for the Assembly of PEMFC Stacks, Machines 7 (2019) 66. https://doi.org/10.3390/machines7040066.

[5] J. Schäfer, H.W. Weinmann, D. Mayer, T. Storz, J. Hofmann, J. Fleischer, Synergien zwischen Batterie- und Brennstoffzellen: Potenzialbewertung anhand von Struktur- und Maschinenparametern in der Fertigung, wt-online 2020 (2020) 735–741.

[6] M. Lanzetta, M. Santochi, G. Tantussi, Computer-Aided Visual Inspection in Assembly, CIRP Annals 48 (1999) 13–16. https://doi.org/10.1016/S0007-8506(07)63121-7.

[7] M. Williams, K. Tignor, L. Sigler, C. Rajagopal, V. Gurau, Robotic Arm for Automated Assembly of Proton Exchange Membrane Fuel Cell Stacks, J. Fuel Cell Sci. Technol 11 (2014) 54501. https://doi.org/10.1115/1.4027392.

[8] R. Kruse, C. Borgelt, C. Braune, F. Klawonn, C. Moewes, M. Steinbrecher, Computational Intelligence, Springer Fachmedien Wiesbaden, Wiesbaden, 2015.

[9] O. Kramer, Computational Intelligence, Springer Berlin Heidelberg, Berlin, Heidelberg, 2009.